American Mineralogist, Volume 74, pages 840–851, 1989

OH substitution in garnets: X-ray and neutron diffraction, infrared, and geometric-modeling studies

GEORGE A. LAGER
Department of Geology, University of Louisville, Louisville, Kentucky 40292, U.S.A.
THOMAS ARMBRUSTER
Laboratory for Chemical and Mineralogical Crystallography, University of Bern, Freiestrasse 3, CH-3012, Bern, Switzerland
FRANK J. ROTELLA
IPNS Division, Argonne National Laboratory, Argonne, Illinois 60439, U.S.A.
GEORGE R. ROSSMAN
Division of Geological and Planetary Sciences, California Institute of Technology, Pasadena, California 91125, U.S.A.

ABSTRACT

Tetrahedral-site occupations were determined for three titanian andradites (San Benito County, California) and a synthetic deuterated hibschite by using X-ray single-crystal and neutron powder data, respectively. Site refinements reveal the presence of tetrahedral vacancies (4–14%) in all three andradites. Infrared absorption spectra measured for the same material used in the X-ray analysis indicate structurally bound water (as OH^-) in amounts of 0.8 to 5.7 wt% OH, which is in good agreement with water contents derived from the refinements. These data confirm that the tetrahedral site is not fully occupied and that charge balance can be achieved by the substitution $(O_4H_4)^{4-} = (SiO_4)^{4-}$. The proton position could not be determined because of the small amount of H present.

Diffraction maxima in the neutron profile for hibschite exhibited small, well-defined shoulders related to chemical inhomogeneity. The data were fit using multiphase Rietveld techniques assuming four phases with slightly different Si/D ratios. Structural parameters [a = 12.0105(3) Å; O(x,y,z) = 0.03561(14), 0.04653(12), 0.64957(12); d site = 0.767(6) Si] refined for the major phase [62(3)% mole fraction) were consistent with X-ray refinements of natural hydrogrossulars. The deuterium atom [0.0965(5), 0.0520(4), 0.6600(5)] was located (ΔF map) outside the tetrahedral volume near the position reported for the Si-free end-member. A significant improvement in R factor was obtained after refinement of a split-atom model to describe the oxygen positional disorder. The short O–D distance [0.744(6)] calculated for the ordered (average) structure can be interpreted within the context of this model.

Distance-least-squares (DLS-76) calculations were used to simulate the effect of the $(O_4H_4)^{4-} = (SiO_4)^{4-}$ substitution on the grossular structure. If the tetrahedral d–O distance, calculated from vacancy concentration, is weighted heavily in the geometric refinement, structural variations in the hydrogrossular series [$Ca_3Al_2(SiO_4)_3$-$Ca_3Al_2(O_4H_4)_3$] can be predicted. Application of DLS to other garnet structures suggests that mantle garnets (rich in pyrope component) may contain only very limited amounts of water.

INTRODUCTION

The substitution of H for Si in grossular garnet was first experimentally verified by Cohen-Addad et al. (1967). Using neutron diffraction and infrared (IR) and nuclear magnetic resonance spectroscopy, it was discovered that in the garnets $Ca_3Al_2(O_4H_4)_3$ and $Ca_3Al_2(SiO_4)_{2.16}(O_4H_4)_{0.84}$, H is present as OH groups and is bonded to oxygen surrounding a tetrahedral vacancy. More recently, X-ray and IR studies have confirmed that the so-called hydrogarnet substitution [$(O_4H_4)^{4-} = (SiO_4)^{4-}$] is not unique to grossular but is also common in other garnets (Aines and Rossman, 1984, 1985; Basso et al., 1984a, 1984b). However, the extent of the OH substitution is apparently related to composition, i.e., pyralspite garnets contain only a limited amount of water (<0.5 wt%) relative to ugrandites (up to 20 wt%).

There has been considerable interest in hydrogarnets recently for several reasons:

1. The fact that garnets contain a hydrous component has important implications with respect to geochemical models derived for the Earth's mantle. For example, water contents of garnets of suspected mantle origin can be used to place constraints on mantle water fugacities (Aines and Rossman, 1984).

0003–004X/89/0708–0840$02.00

2. Hickmott et al. (1987) have used trace-element zoning in garnets to investigate *P-T* paths in metamorphic environments. H zonation in hydrogrossular, a fairly common metamorphic mineral, may also be an important source of information about the metamorphic processes that occur during crystal growth.

3. A number of studies have focused on the effect of OH on the deformation of olivine (see, for example, Justice and Graham, 1982). Although garnet and olivine are commonly associated in peridotite xenoliths, very little is known about the effect of H on the elastic properties of garnet.

The present study was carried out to address a number of questions that pertain to hydrogarnet crystal chemistry. To date, no neutron-diffraction data had been collected for an intermediate member of the hydrogrossular series.[1] Armbruster and Lager (1989) in a recent paper could find no relationship between the H position and OH content in the hydrogrossular series. This proposal was based on a re-examination of the plazolite $[Ca_3Al_2(SiO_4)_{1.53}(O_4H_4)_{1.47}]$ (Basso et al., 1983) and katoite $[Ca_3Al_2(SiO_4)_{0.64}(O_4H_4)_{2.36}]$ (Sacerdoti and Passaglia, 1985) structures using structural amplitudes from the original X-ray studies. In the same paper, it was also shown that the oxygen positional disorder could be described in terms of two slightly displaced oxygen sites that correspond in position to the sites in anhydrous grossular and Si-free katoite. In this study, neutron powder-diffraction data were collected for a synthetic deuterated hibschite $[Ca_3Al_2(SiO_4)_{2.30}(O_4D_4)_{0.70}]$ to determine a more accurate D(H) position and to test the split-atom model based on X-ray diffraction data. Neutron diffraction is well-suited to this problem because of its sensitivity to both D and oxygen, which are the strongest neutron scatterers in the hydrogrossular structure.

Titanian andradites (melanites) have been the subject of a number of spectroscopic studies in recent years (Dowty, 1971; Huggins et al., 1977; Huggins, 1977; Schwartz et al., 1980; Waychunas, 1987). Although the Si deficiency in these garnets is well known, it has not been related to the presence of tetrahedral vacancies in the structure. Rather, it has been proposed that Fe^{3+}, Al^{3+}, or perhaps Ti^{4+} may occupy the tetrahedral sites in order to maintain charge balance. The crystal chemistry of hydrous grossular-andradites with reported water and TiO_2 contents (electron-microprobe and wet-chemical analyses) ranging from 1 to 3.43 wt% H_2O and from 0.08 to 3.03 wt% TiO_2 has also been investigated (Basso et al., 1981; Basso et al., 1984a, 1984b). On the basis of single-crystal X-ray studies, Basso et al. (1984a, 1984b) proposed a more general hydrogarnet substitution in which H may also substitute for cations in the X (dodecahedral) and Y (octahedral) sites. According to Birkett and Trzcienski (1984), chemical formulae calculated from electron-microprobe analyses also require a multi-site OH substitution in hydrospessartine-hydroandradite solid solutions.

To learn more about the nature and extent of the OH substitution in natural garnets, X-ray single-crystal and IR absorption data were collected for three titanian andradites (San Benito County, California). In addition, distance-least-squares (DLS) methods were used to simulate the effect of the OH substitution on the garnet structure. Of particular interest is the apparent relationship between OH content and garnet composition.

Experimental procedure

Representative electron-microprobe (EM) analyses and chemical formulae for the andradite garnets are given in Table 1. Mineral compositions were determined using an automated, combined wavelength-dispersive and energy-dispersive microprobe system (ARL-SEMQ and Tracer Northern 2000). An acceleration potential of 15 kV, a sample current of 20 nA measured on brass, and a beam size of approximately 3 μm were used. Natural and synthetic oxides and silicates were used as standard materials. The raw data were corrected for drift, deadtime, and background. Matrix corrections were calculated using a ZAF correction procedure. Analyses 1–3 were obtained from a large single crystal (~200 μm in diameter), part of which was used in the X-ray diffraction experiment (crystal SB-3). Analyses 4–8 were obtained from the same thin section as X-ray crystals SB-1 and SB-2. These crystals were lost during grinding prior to the EM analysis. Samples SB-1 and SB-2 were collected near stop 5 (San Benito County) on the International Mineralogical Association field trip to the New Idria area, California (Coleman, 1986). Sample SB-3 is from a nearby locality on the south slope of Santa Rita Peak, San Benito County. These andradites occur in a calc-silicate body that formed by metasomatic replacement of serpentine.

The X-ray diffraction data (Table 2)[2] were collected at room temperature with an Enraf-Nonius CAD-4 diffractometer (graphite-monochromatized Mo$K\alpha$ radiation) following the procedures outlined by Lager et al. (1987). Data reduction, including background and Lorentz-polarization corrections, was carried out using the SDP (Enraf-Nonius, 1983) program library. The program PROMETHEUS (Zucker et al., 1983) was used with neutral-atom scattering factors (corrected for the effects of anomalous

[1] In the new nomenclature approved by the International Mineralogical Association, members of this series with a grossular (Gr) component ≥ 50% are called *hibschites* whereas those with Gr < 50% are referred to as *katoites* [including the Si-free end-member $Ca_3Al_2(O_4H_4)_3$]. OH-containing grossulars for which the value of x has not been determined are collectively referred to as *hydrogrossulars* (Passaglia and Rinaldi, 1984). Although the garnet described by Basso et al. (1983) would be classified as a hibschite, the mineral name *plazolite* is retained for this particular sample because of its common usage in the literature (Foshag, 1920; Pabst, 1937).

[2] To obtain copies of Tables 2 and 3, order Document AM-89-411 from the Business Office, Mineralogical Society of America, 1625 I Street, N.W., Suite 414, Washington, D.C. 20006, U.S.A. Please remit $5.00 in advance for the microfiche.

TABLE 1. Representative electron-microprobe analyses and chemical formulae for San Benito andradites

	Analysis number							
	1	2	3	4	5	6	7	8
SiO_2	33.99	32.79	33.78	34.78	34.72	34.54	33.57	35.49
TiO_2	1.32	2.10	1.51	2.51	5.77	4.48	3.95	0.35
Al_2O_3	1.48	1.56	1.18	4.70	3.23	1.42	1.49	3.69
Cr_2O_3	0.08	0.00	0.00	0.19	0.13	0.07	0.00	0.15
MgO	0.36	0.57	0.30	0.00	0.00	0.00	0.00	0.00
Fe_2O_3	25.82	25.44	25.85	19.49	20.51	22.45	22.87	24.89
Na_2O	0.00	0.14	0.00	0.00	0.00	0.00	0.00	0.00
K_2O	0.03	0.07	0.01	0.00	0.00	0.00	0.00	0.00
CaO	33.64	33.10	33.45	35.67	33.79	33.77	34.83	33.05
	Mineral formulae: [Ca + Fe + Al + Ti + Cr + Mg + Na + K] = 5							
Si	2.89	2.77	2.90	2.88	2.90	2.97	2.83	3.01
Ti	0.08	0.13	0.10	0.16	0.36	0.29	0.25	0.02
Al	0.15	0.16	0.12	0.46	0.32	0.14	0.15	0.37
Cr	0.01	0.00	0.00	0.01	0.01	0.01	0.00	0.01
Mg	0.05	0.07	0.04	0.00	0.00	0.00	0.00	0.00
Fe^{3+}	1.65	1.62	1.63	1.21	1.29	1.45	1.45	1.59
Na	0.00	0.02	0.00	0.00	0.00	0.00	0.00	0.00
K	0.01	0.01	0.01	0.00	0.00	0.00	0.00	0.00
Ca	3.06	2.99	3.00	3.16	3.02	3.11	3.15	3.01

scattering) for the least-squares refinements. Analysis of difference-Fourier maps failed to reveal the position of the H atom.

In addition to positional and anisotropic displacement parameters,[3] site occupancies were refined, allowing for Si and vacancies on the tetrahedral site and Fe and Al on the octahedral site. Previous refinements and EM analyses indicated that the dodecahedral site was totally occupied by Ca. The Ti content of andradites from the same thin section as crystals SB-1 and SB-2 varied significantly from rim to core and from crystal to crystal. Crystal SB-3 was fairly homogeneous with 0.08–0.13 Ti atoms per formula unit. In all cases, Ti was assumed to occupy the octahedral site; significant amounts of tetrahedrally coordinated Ti were not considered, in agreement with the low scattering power observed at the tetrahedral position. Because of the variation in Ti content within the sample and the similarity of X-ray scattering factors for Fe and Ti (in contrast to Al), the Ti content was included in the refined Fe population (Fe + Ti).

The polycrystalline sample of hibschite (~3 cm^3) was synthesized hydrothermally from a mixture of 1 mol of Si-free katoite [$Ca_3Al_2(O_4D_4)_3$] (Lager et al., 1987) and 2 mol of amorphous SiO_2 (2 months, 623 K, 500 bars) (Lager et al., 1988). Grinding and mixing in a N_2 atmosphere were carried out periodically during the synthesis to achieve homogeneity. In spite of these precautions, diffraction maxima in the neutron profile (Fig. 1) exhibited small, well-defined shoulders related to compositional gradients involving Si and D (not unlike those observed in natural hydrogrossulars, e.g., pink Transvaal "jade"; Zabinski, 1966). These additional reflections were not visible in Debye-Scherrer (Cu$K\alpha$ radiation, 114-mm-diameter camera) photographs and could be observed only in long-exposure (12 h) Guinier X-ray (Fe$K\alpha$ radiation) films.

The neutron data (Table 3; see footnote 2) were collected at room temperature on the General Purpose Powder Diffractometer (GPPD) at Argonne National Laboratory's Intense Pulsed Neutron Source (IPNS). The data ($2\theta = \pm 90°$) were fit using the time-of-flight (Von Dreele et al., 1982) Rietveld method (Rietveld, 1969) for multiple-phase samples (Rotella and Richardson, 1986; Rotella, 1986). In the Rietveld method, parameters that describe the crystal structure, as well as those describing the shape of the diffraction maxima, can be adjusted by least-squares methods until the best fit is obtained between the observed spectrum and that calculated from the model. In this case, it was necessary to describe the scattering by assuming a four-phase model, with each phase differing slightly in Si/D ratio. (An unidentifiable impurity phase was also observed in the Guinier photograph. The sharpness of the diffraction lines attributed to this phase relative to those from synthetic hibschite facilitated identification of three impurity peaks in the neutron spectrum and exclusion of these peaks from the subsequent Rietveld analysis.) Due to the complex nature of the spectrum, values for unit-cell and peak-shape parameters for each phase were determined by individual least-squares fits to several quartets in the profile (FORTRAN program TOFMANY; Faber and Hitterman, 1986). Broad features attributed primarily to scattering from amorphous SiO_2 were observed in the neutron data during Rietveld analysis. This noncrystalline scattering component was fit using a Fourier-filtering technique and removed from the raw data prior to subsequent least-squares refinement (Richardson and Faber, 1986).

The relative mole fractions of the four phases in the polycrystalline sample are given in Table 4. Because phase 2 (see Table 4) is much more abundant than any of the

[3] The use of the term "displacement parameter" rather than "vibration parameter" or "thermal parameter" is preferred because the mean-square displacement of an atom may reflect static or dynamic disorder as well as true thermal motion (Dunitz et al., 1988).

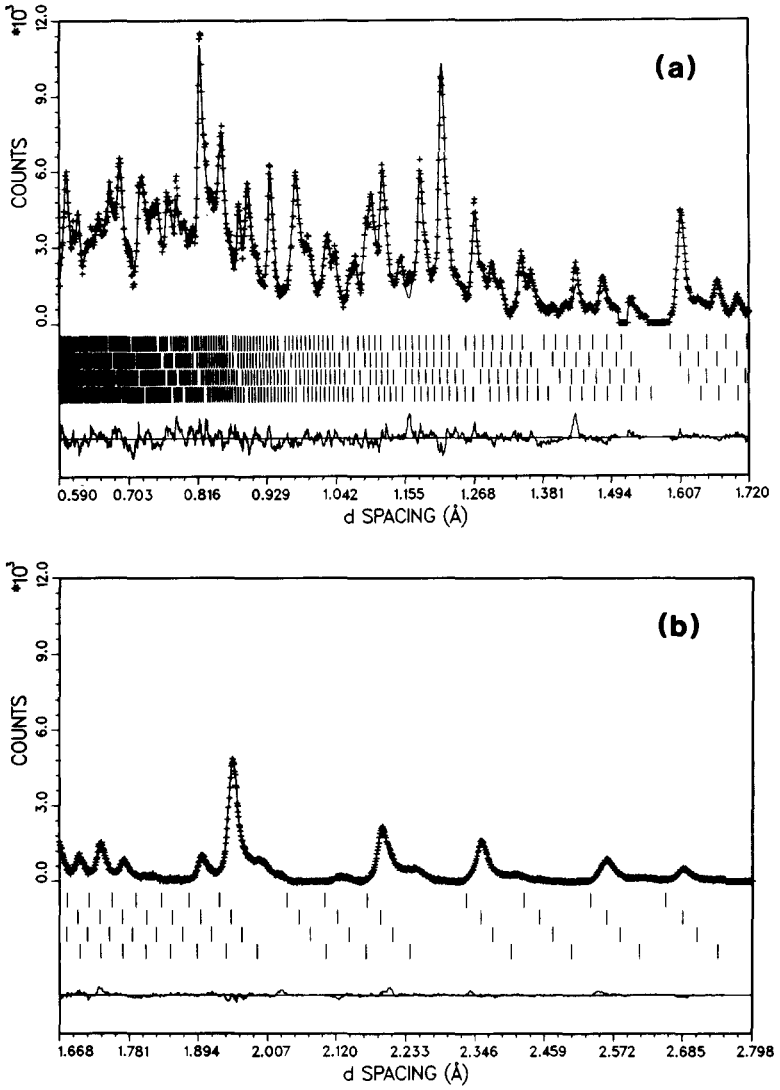

Fig. 1. Rietveld refinement profile for synthetic hibschite $[Ca_3Al_2(SiO_4)_{2.30}(O_4H_4)_{0.70}]$ at room temperature. Plus marks represent the observed data. Solid line is the best-fit profile. Tick marks below the profile indicate the positions of all allowed reflections for each of the four phases. A difference curve appears at the bottom. Background was fit as part of the refinement but has been subtracted before plotting. Two *d* regions near 1.51 Å and one near 2.10 Å were excluded from the refinement due to the presence of an unidentifiable impurity phase.

other phases, it was not possible to refine simultaneously the structural parameters of all four phases. However, the structural similarity among the phases allowed for the construction of a constrained model consistent with hydrogarnet crystal chemistry. In this model, a scale factor, unit-cell parameter, and absorption parameter were refined for each phase independently in the Rietveld analysis; isotropic displacement parameters for all atoms in the minor phases were constrained to vary as their analogues in phase 2. The oxygen position in phase 2 was refined independently, whereas that in each of the minor phases was determined from the known variation of the positional parameters of oxygen with unit-cell parameter in the hydrogrossular series. A similar constraint was applied to the Si occupation for each of the minor phases; the Si occupation of phase 2 was refined independently.

The D atom was located by difference-Fourier synthesis (Fig. 2) outside the tetrahedral volume near the position reported for Si-free katoite (Lager et al., 1987). The D position (and isotropic displacement parameter) was included in the model for all phases. D was varied independently in phase 2 and, in the minor phases, constrained to the phase 2 values. The value for D occupation of phase 2 was constrained based on the refined Si value.

Attempts to refine an isotropic displacement parameter for the tetrahedral site resulted in a negative value within 2 to 3 esd's of zero. This could reflect an incorrect tetrahedral-site occupation; however, the refined site occupation (Si) for the major phase was consistent with the unit-cell parameter (Passaglia and Rinaldi, 1984, Fig. 6) and with results obtained from X-ray refinements of natural hydrogrossulars (Basso et al., 1983; Sacerdoti and Passaglia, 1985). In subsequent refinements, the Si displacement parameter was fixed at 0.30 $Å^2$ (plazolite, Basso et al., 1983) for all phases. This constraint did not produce a significant change in the Si occupation of phase 2.

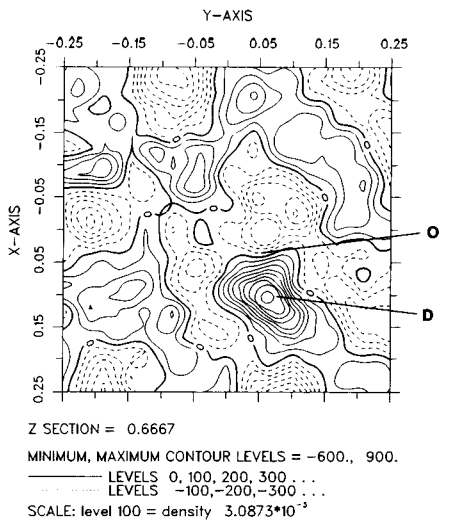

Fig. 2. Difference-Fourier section (z = 0.6667) showing the location of the oxygen (O) and deuterium (D) atoms in synthetic hibschite (neutron-scattering density in units of $cm^{-12}/Å^3$). The map is based on a refinement with isotropic displacement parameters.

Data-collection and refinement parameters for the neutron and X-ray experiments are summarized in Table 4. Atomic and displacement parameters, site occupations, and interatomic distances and angles for the major hydrogrossular phase (phase 2) are collected in Tables 5 and 6. The corresponding data for the three andradite refinements are presented in Tables 7, 8, and 9.

A split-atom model for the oxygen position was refined also for phase 2 (R_{wp} = 2.491% for 33 variables). The refined values for the oxygen positions and displacement parameters in grossular and Si-free katoite are, respectively, [0.0392(2), 0.0445(3), 0.6514(2); 0.31(4) Å²] and [0.0223(7), 0.0545(9), 0.6415(8); 0.55(12) Å²]. The occupations of the oxygen sites were constrained to the refined Si occupation. The Hamilton R-factor ratio indicated that for this model to be preferred statistically over the oxygen-ordered model (R_{wp} = 2.568% for 29 variables) at a 99.5% level of confidence, R_{wp} must be reduced by *at least* a factor of ($R_{b=4,N=1964,\alpha=0.005}$) 1.0038 (see Table 4.2, p. 288–292; *International Tables for X-ray Crystallography,* 1974). The observed R-factor ratio was 1.0309, indicating that the split-oxygen model is preferred at a 99.5% confidence level. The oxygen-ordered (average)

Table 4. Data-collection and refinement parameters for synthetic hibschite (neutron) and titanian andradite (X-ray)

	Space group: $Ia\bar{3}d$ (O_h^{10}; no. 230)			
	Neutron: GPPD; $2\theta = \pm 90°$; room temperature			
	Scattering lengths* (10^{-12} cm): b(Ca) = 0.490			
		b(Al) = 0.345		
		b(Si) = 0.4149		
		b(O) = 0.5803		
		b(D) = 0.667		
	Phase 1	Phase 2	Phase 3	Phase 4
a (Å)	11.888(3)	12.0105(3)	12.117(2)	12.268(2)
V (Å³)	1680.2(11)	1732.56(13)	1779.2(7)	1846.3(10)
Scale factor	0.0042(9)	0.092(3)	0.0109(10)	0.036(2)
Mole fraction (%)**	2.6 ± 0.4	62.0 ± 2.6	7.8 ± 0.8	27.6 ± 1.7
R_{F^2} (%)†	6.10	4.32	4.92	3.84
R_{wp} (%)†		2.57		
R_{exp} (%)†		1.19		
d range (Å)		0.59–2.80		
Number of observations		1997		
Number of variables		29		
Number of reflections	421	437	449	477

X-ray: Enraf-Nonius CAD-4; Mo$K\alpha$ radiation; room temperature

	SB-1	SB-2	SB-3
Scan mode	ω	ω	ω
θ limit (°)	35	30	35
Variation in standards (%)	3	3	3
Crystal size (μm)	120 × 120 × 120	180 × 180 × 220	180 × 230 × 250
Absorption correction	none	none	empirical
Agreement on intensity (%)	1.8	2.0	2.7
Accepted reflections	189	164	202
Rejected reflections < $6\sigma(F_o)$	110	55	129
Number of variables	19	19	19
R_F (%)‡	1.2	1.3	2.7
R_{wF} (%)‡	1.8	2.2	3.0

Note: In this and subsequent tables, estimated standard deviations are in parentheses and refer to the last decimal place cited.
* Values from compilation of Sears (1986).
** Hill and Howard (1987).
† Refer to Jorgensen et al. (1989) for definition of R factors.
‡ $R_F = \Sigma||F_o| - |F_c||/\Sigma|F_o|$; $R_{wF} = [w(|F_o| - |F_c|)^2/\Sigma w|F_o|^2]^{1/2}$.

TABLE 5. Atomic parameters and stoichiometry for average hibschite structure

Atom	x	y	z	B_{iso} (Å²)	Stoichiometry
O	0.03561(14)	0.04653(12)	0.64957(12)	0.64(4)	12.00
Ca	0	1/4	1/8	0.47(5)	3.00
Al	0	0	0	0.66(7)	2.00
Si	3/8	0	1/4	0.30*	2.300(17)
D	0.0965(5)	0.0520(4)	0.6600(5)	1.71(14)	2.800**

* Attempts at refining B_{iso} for Si resulted in negative values within 2–3 esd's of zero. Subsequently, B_{iso} for Si was fixed at 0.30 throughout the analysis.

** The D stoichiometry was set equal to 12 − 4 times the Si stoichiometry throughout the analysis.

structure is reported in Tables 5 and 6 to facilitate comparison with observed and DLS-generated structures.

RESULTS AND DISCUSSION

Synthetic hibschite

The hydrogrossular defect structure can be represented in terms of the formula $^{[8]}Ca_3\ ^{[6]}Al_2(^{[4]}SiO_4)_{3-x}(O_4H_4)_x$ where $x = 0$ refers to anhydrous grossular garnet and $x = 3$ refers to Si-free katoite. Superscripts in brackets refer to the three different types of cation environments in the structure: the eight-coordinated dodecahedral (X) site, the six-coordinated octahedral (Y) site, and the tetrahedral (Z) site (Fig. 3). The substitution $(O_4H_4)^{4-} = (SiO_4)^{4-}$ is the proposed mechanism for incorporating H in the structure and creating an H-associated point defect (vacancy) at the tetrahedral site. With one exception, the H atom lies outside the oxygen tetrahedron in all hydrogrossulars examined to date (Fig. 4). Prior to this study, only one of these structures (Si-free katoite, Lager et al., 1987) had been refined by state-of-the-art neutron-diffraction techniques.

The O–D distance reported for hibschite (0.744(6) Å, Table 6) is anomalously short compared to other O–D distances determined by neutron-diffraction methods (mean value 0.969(1) Å; Ceccarelli et al., 1981). In the X-ray structure of katoite $[Ca_3Al_2(SiO_4)_{0.64}(O_4H_4)_{2.36}]$, Sacerdoti and Passaglia (1985) rationalized the short O–H distance (0.65 Å) in terms of positional disorder of oxygen, i.e., oxygen will occupy two different sites depending upon whether the tetrahedron is occupied by Si or vacant. The X-ray refinement, in this case, will yield an average oxygen position that represents the superposition of two sites. The positional disorder should be a rather significant effect judging from a comparison of the *d*–O distances (= Si–O distance in anhydrous silicate garnets, Table 6) in grossular (1.64 Å), and Si-free katoite (1.95 Å). Sacerdoti and Passaglia (1985) were unable to refine a split-atom model to describe the oxygen disorder. More recently, Armbruster and Lager (1989) have refined a split-oxygen model for both plazolite and katoite using the structural amplitudes from the original X-ray studies (Basso et al., 1983; Sacerdoti and Passaglia, 1985). The synthetic-hibschite structure can also be described in terms of two slightly displaced (0.264 Å) oxygen sites that correspond in position to the sites in grossular [0.03808(11), 0.04493(11), 0.65140(9)] (Novak and Gibbs, 1971) and Si-free katoite [0.0288(2), 0.0522(1), 0.6402(1)] (Lager et al., 1987). The O–O displacement vector is approximately parallel (with-

TABLE 6. Interatomic distances (Å) and angles (°) for average hibschite structure

Tetrahedron			
d–O*	1.709(2)		
2 O(1)–O(2)	2.659(3)	O(1)–Si–O(2)	102.15(10)
4 O(1)–O(3)	2.854(3)	O(1)–Si–O(3)	113.25(5)
Mean	2.789		
Octahedron			
Al–O	1.929(2)		
6 O(1)–O(4)	2.730(3)	O(1)–Al–O(4)	90.05(7)
6 O(1)–O(5)	2.727(3)	O(1)–Al–O(5)	89.95(7)
Mean	2.728		
Dodecahedron			
4 Ca(1)–O(4)	2.343(2)		
4 Ca(2)–O(4)	2.498(2)		
Mean	2.420		
2 O(1)–O(2)	2.659(3)	O(1)–Ca(2)–O(2)	69.15(8)
4 O(1)–O(4)	2.730(3)	O(1)–Ca(2)–O(4)	68.56(7)
4 O(1)–O(7)	3.506(1)	O(1)–Ca(2)–O(7)	92.75(5)
4 O(4)–O(6)	2.982(3)	O(4)–Ca(2)–O(6)	75.97(6)
2 O(4)–O(7)	2.912(3)	O(4)–Ca(2)–O(7)	71.28(7)
2 O(7)–O(8)	4.104(3)	O(7)–Ca(2)–O(8)	110.42(7)
Mean	3.123		
O–D	0.744(6)		
d–D	1.295(6)		
Al–D	2.329(6)		
Ca(1)–D	2.938(5)		
Ca(2)–D	2.678(5)		

* *d* is Wyckoff notation for site with point symmetry $\bar{4}$ in space group *Ia3d*.

TABLE 7. Unit-cell and oxygen parameters, U_{eq} values (Å²), and site occupations for San Benito (SB) andradites

		SB-1	SB-2	SB-3
a		12.057(2)	12.085(2)	12.106(2)
X	Ca	1.0	1.0	1.0
	U_{eq}†	0.523(6)	0.546(7)	0.597(6)
Y	(Fe, Al)	0.841(5)	0.752(6)	0.798(5)
	U_{eq}	0.346(2)	0.360(4)	0.411(3)
Z	(Si, vacancy)	0.960(5)	0.915(5)	0.860(5)
	U_{eq}	0.29(1)	0.20(1)	0.23(1)
O	*x*	0.03923(9)	0.03880(9)	0.0387(1)
	y	0.04842(8)	0.04845(8)	0.04860(9)
	z	0.65500(8)	0.65454(8)	0.65441(9)
	U_{eq}	0.54(2)	0.60(2)	0.69(2)

† $U_{eq} = (8/3)\pi^2\Sigma_i(\Sigma_j U_{ij} a_i^* a_j^* a_i a_j)$ where $\sigma(U_{eq})$ is calculated from expression of Schomaker and Marsh (1983).

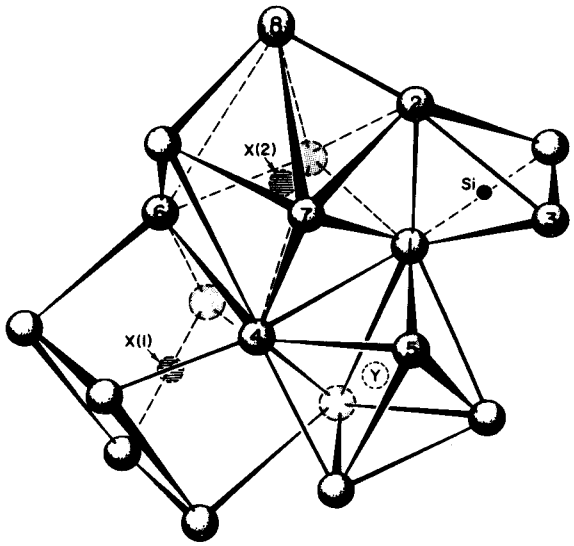

Fig. 3. A portion of the garnet structure showing the three different types of polyhedra and the numbering scheme for the atoms (Novak and Gibbs, 1971). In end-member andradite and grossular, X(1) and X(2) refer to Ca^{2+}, and Y represents Fe^{3+} and Al^{3+}.

in 18°) to the tetrahedral *d*–O direction, as defined by the average oxygen position in the ordered model. This is consistent with the observation that in the hydrogrossular series, the tetrahedron changes dramatically in size but not in shape or orientation (i.e., only a small rigid-body rotation). The magnitude of the displacement reflects the relative difference in the *d*–O distances for grossular and Si-free katoite. It should be noted that the oxygen (Si-free katoite) position is characterized by a larger esd because of the lower relative occupation of this site (23%). Within the context of the oxygen-disordered model, a reasonable O–D distance (0.982 Å) is obtained by using the above oxygen position and assuming a = 12.5695 Å (as in Si-free katoite). The D position (Table 5) is near that reported for Si-free katoite [0.0983(1), 0.0485(1), 0.6587(2)], indicating that the location of the D(H) atom is not strongly dependent on OH content.

TABLE 8. Anisotropic displacement parameters ($\times 10^4$) for San Benito (SB) andradites

Atom	U_{11}†	U_{22}	U_{33}	U_{12}	U_{13}	U_{23}
SB-1						
X	75(2)	75	48(3)	15(2)	0	0
Y	44(1)	44	44	−2(1)	−2	−2
Z	35(4)	38(3)	38	0	0	0
O	66(5)	75(5)	64(5)	1(3)	2(3)	1(4)
SB-2						
X	79(2)	79	49(3)	21(2)	0	0
Y	46(2)	46	46	2(1)	2	2
Z	21(5)	28(4)	28	0	0	0
O	90(5)	72(6)	68(5)	−8(4)	15(4)	−6(4)
SB-3						
X	86(2)	86	55(3)	24(2)	0	0
Y	52(2)	52	52	4(1)	4	4
Z	26(4)	30(3)	30	0	0	0
O	102(5)	83(5)	77(5)	−8(4)	17(4)	−7(4)

† $T = \exp[-2\pi^2(U_{11}h^2a^{*2} + U_{22}k^2b^{*2} + U_{33}l^2c^{*2} + 2U_{12}hka^*b^* + 2U_{13}hla^*c^* + 2U_{23}klb^*c^*]$.

TABLE 9. Interatomic distances (Å) and angles (°) for San Benito andradites

	SB-1	SB-2	SB-3
Tetrahedron			
d–O	1.650(1)	1.661(1)	1.666(1)
2 O(1)–O(2)	2.571(2)	2.587(2)	2.596(2)
4 O(1)–O(3)	2.754(2)	2.773(2)	2.781(2)
Mean	2.693	2.711	2.719
2 O(1)–Si–O(2)	102.37(6)	102.32(6)	102.35(6)
4 O(1)–Si–O(3)	113.13(5)	113.16(5)	113.15(5)
Octahedron			
Al–O	2.014(1)	2.013(1)	2.015(1)
6 O(1)–O(4)	2.873(2)	2.866(2)	2.868(2)
6 O(1)–O(5)	2.824(2)	2.826(2)	2.831(2)
Mean	2.849	2.846	2.850
6 O(1)–Al–O(4)	90.98(4)	90.80(4)	90.73(5)
6 O(1)–Al–O(5)	89.03(5)	89.20(5)	89.27(5)
Dodecahedron			
4 Ca(1)–O(4)	2.361(1)	2.365(1)	2.369(1)
4 Ca(2)–O(4)	2.502(1)	2.506(1)	2.508(1)
Mean	2.432	2.436	2.439
2 O(1)–O(2)	2.571(2)	2.587(2)	2.596(2)
4 O(1)–O(4)	2.873(2)	2.866(2)	2.868(2)
4 O(1)–O(7)	3.487(2)	3.497(2)	3.504(2)
4 O(4)–O(6)	2.941(2)	2.948(2)	2.951(2)
2 O(4)–O(7)	2.861(2)	2.872(2)	2.875(2)
2 O(7)–O(8)	4.169(2)	4.169(2)	4.172(2)
Mean	3.134	3.139	3.143
2 O(1)–Ca(2)–O(2)	65.99(4)	66.30(4)	66.46(4)
4 O(1)–Ca(2)–O(4)	72.35(4)	72.03(4)	71.96(4)
4 O(1)–Ca(2)–O(7)	91.56(4)	91.73(4)	91.80(4)
4 O(4)–Ca(2)–O(6)	74.35(4)	74.42(4)	74.40(4)
2 O(4)–Ca(2)–O(7)	69.74(3)	69.91(3)	69.94(3)
2 O(7)–Ca(2)–O(8)	112.84(4)	112.58(4)	112.54(4)

Polyhedral distances for synthetic hibschite and four other garnets in the hydrogrossular series are compared in Figure 5. Major structural variations with OH substitution can be summarized as follows: (1) The tetrahedra increase in size from *d*–O = 1.64 Å (grossular) to *d*–O = 1.95 Å [Si-free katoite]. (2) The shared octahedral edge [O(1)–O(4)] decreases in length whereas the unshared edge [O(1)–O(5)] increases. The Al–O distance remains essentially constant. For the composition synthesized in this study [$Ca_3Al_2(SiO_4)_{2.30}(O_4D_4)_{0.70}$], the octahedron is characterized by a very small degree of distortion. (3) The Ca(1)–O(4) distance increases at a much greater rate than the Ca(2)–O(4) distance.

Using the distance-least-squares (DLS) method (Baerlocher et al., 1977), Meagher (1975) was able to show that the response of the garnet structure to chemical substitution can be largely interpreted in terms of a geometrical model. In this study, the DLS method was used to simulate the effect of the hydrogarnet substitution [$(O_4H_4)^{4-} = (SiO_4)^{4-}$] on the grossular structure. The DLS program is based on the observation that the total number of crystallographically independent interatomic distances in a crystal structure generally exceed the number of atomic coordinates and unit-cell parameters. If a suf-

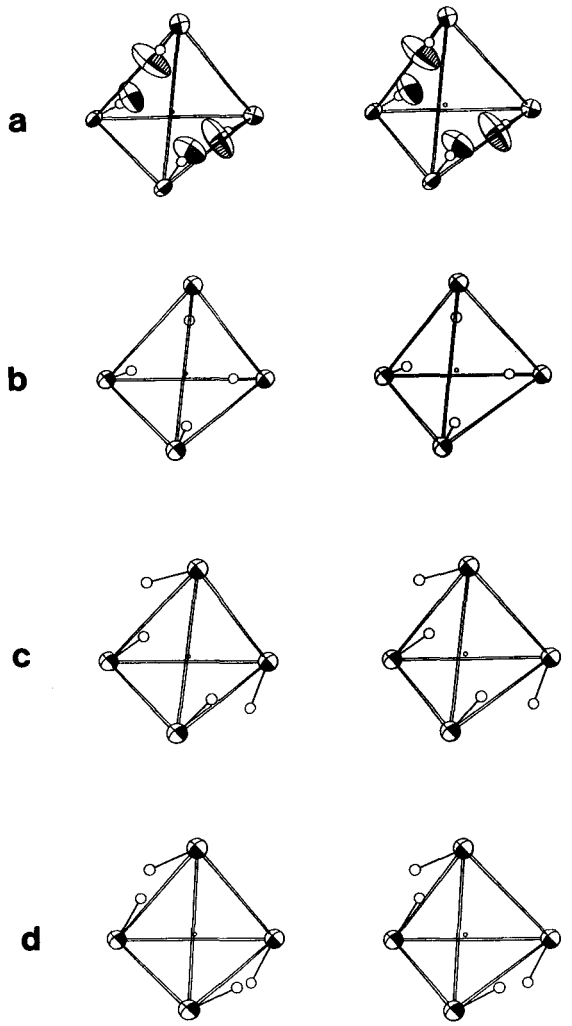

Fig. 4. Stereo ORTEP plots of atomic environment about the $\bar{4}$ site (*d* position) showing the oxygen tetrahedron with associated hydrogens (deuteriums). (**a**) Neutron refinement of Si-free katoite $Ca_3Al_2(O_4D_4)_3$ at 300 K; open circles along O–D vector represent H positions from X-ray refinement. (**b**) Katoite $Ca_3Al_2(SiO_4)_{0.64}(O_4H_4)_{2.36}$ (Sacerdoti and Passaglia, 1985). (**c**) Plazolite $Ca_3Al_2(SiO_4)_{1.53}(O_4H_4)_{1.47}$ (Basso et al., 1983). (**d**) Synthetic $Ca_3Al_2(SiO_4)_{2.16}(O_4H_4)_{0.84}$ (Cohen-Addad et al., 1967). In b–d, a constant diameter for oxygen and H spheres is used. The D position for synthetic hibschite is near that shown for Si-free katoite (a) (modified from Lager et al., 1987).

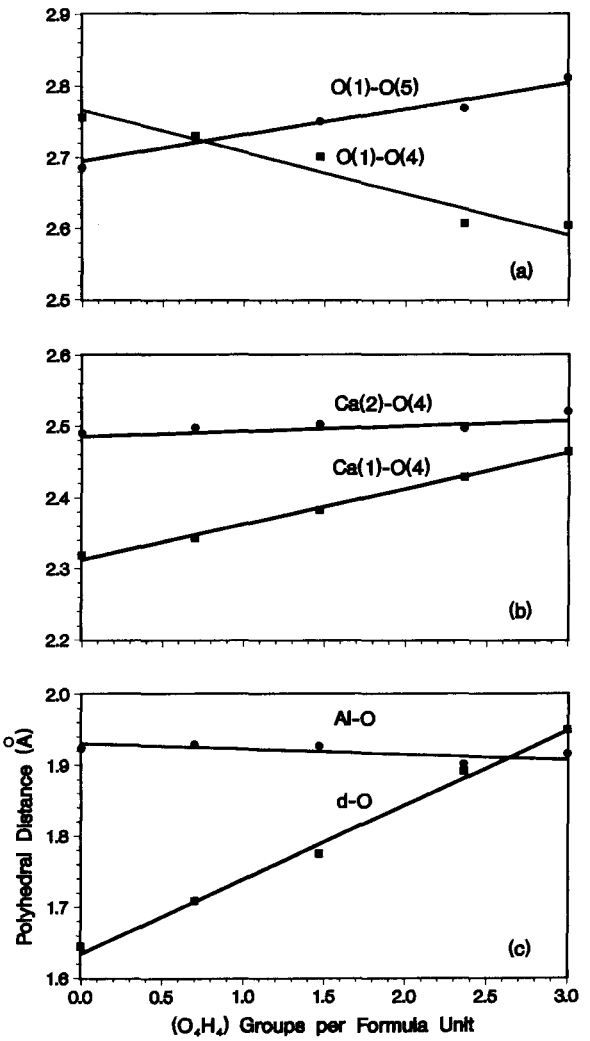

Fig. 5. Number of (O_4H_4) groups per formula unit, as defined by x in the hydrogarnet formula $[Ca_3Al_2(SiO_4)_{3-x}(O_4H_4)_x]$, plotted as a function of polyhedral distance for garnets in the hydrograssular series. The shared and unshared octahedral edges are denoted as O(1)–O(4) and O(1)–O(5), respectively. The lines through the data represent unweighted least-squares fits. Data are from the following sources: $x = 0.0$, grossular, Novak and Gibbs (1971); $x = 0.70$, synthetic hibschite, this study; $x = 1.47$, plazolite, Basso et al. (1983); $x = 2.36$, katoite, Sacerdoti and Passaglia (1985); $x = 3.0$, Si-free katoite, Lager et al. (1987). Errors associated with the distances are equal to or smaller than the size of the symbols.

ficient number of distances are "prescribed" by the user, atomic coordinates and unit-cell parameters can be estimated by least-squares procedures. The function minimized is of the form

$$\sum_j w_j^2[D_j^o - D_j^c]^2,$$

where D_j^o and D_j^c refer to the prescribed and calculated distances and w_j is the weight. DLS refinements of grossular and hydrogrossular can be compared to determine how the observed grossular structure may respond to changes in the size, shape, and orientation of constituent polyhedra, e.g., the expansion of the tetrahedra with OH substitution. In short, DLS is a form of model building

TABLE 10. Results of DLS calculations

	d–O	Y–O	X(1)–O(4)	X(2)–O(4)	O(1)–O(4)*	O(1)–O(5)**	O(1)–O(2)†	O(1)–O(3)‡	O(4)–O(7)§
				Grossular					
Prescribed	1.64	1.91	2.50	2.50	2.70	2.70	2.68	2.68	2.89‖
Refined	1.64	1.93	2.37	2.47	2.79	2.67	2.62	2.71	2.75
Observed	1.645(1)	1.924(1)	2.319(1)	2.490(1)	2.756(2)	2.686(2)	2.567(2)	2.745(1)	2.866(1)
				Plazolite (5.88 OH)					
Prescribed	1.78	1.91	2.50	2.50	2.70	2.70	2.91	2.91	2.88
Refined	1.79	1.92	2.42	2.47	2.69	2.73	2.85	2.96	2.85
Observed	1.775(1)	1.927(1)	2.383(1)	2.503(1)	2.701(2)	2.750(2)	2.775(2)	2.957(2)	2.931(2)
				Katoite (9.44 OH)					
Prescribed	1.89	1.91	2.50	2.50	2.70	2.70	3.09	3.09	2.88
Refined	1.89	1.91	2.45	2.47	2.63	2.79	2.99	3.13	2.92
Observed	1.892(2)	1.902(2)	2.429(1)	2.497(3)	2.607(2)	2.769(3)	2.969(2)	3.147(2)	2.977(3)
				Si-free katoite (12 OH)					
Prescribed	1.95	1.91	2.50	2.50	2.70	2.70	3.18	3.18	2.88
Refined	1.95	1.92	2.48	2.50	2.61	2.82	3.08	3.24	2.98
Observed	1.950(2)	1.916(2)	2.464(2)	2.521(2)	2.604(2)	2.811(2)	3.058(2)	3.245(2)	3.030(2)
				Pyrope					
Prescribed	1.64	1.91	2.27	2.27	2.70	2.70	2.68	2.68	2.75‖
Refined	1.64	1.90	2.21	2.32	2.63	2.75	2.52	2.76	2.75
Observed	1.634(1)	1.886(1)	2.196(2)	2.342(2)	2.617(3)	2.716(2)	2.494(2)	2.751(3)	2.782(3)
				Pyrope (4 OH)					
Prescribed	1.74	1.91	2.27	2.27	2.70	2.70	2.85	2.85	2.75‖
Refined	1.74	1.92	2.25	2.29	2.58	2.85	2.68	2.93	2.75
				Andradite					
Prescribed	1.64	2.03	2.50	2.50	2.86	2.86	2.68	2.68	2.89‖
Refined	1.64	2.01	2.42	2.49	2.91	2.79	2.63	2.70	2.75
Observed	1.643(2)	2.024(2)	2.366(2)	2.500(2)	2.890(3)	2.834(4)	2.564(4)	2.739(3)	2.847(4)
				Andradite (4 OH)					
Prescribed	1.74	2.03	2.50	2.50	2.86	2.86	2.85	2.85	2.88
Refined	1.74	2.03	2.42	2.47	2.85	2.90	2.74	2.89	2.83

Note: Prescribed cation-oxygen distances were calculated from the sum of ionic radii. Oxygen-oxygen distances were then computed from each cation-oxygen distance assuming undistorted polyhedra. Results for anhydrous grossular and pyrope are from Meagher (1975). Observed data are from the following sources: grossular, andradite, and pyrope—Novak and Gibbs (1971); plazolite—Basso et al. (1983); katoite—Sacerdoti and Passaglia (1985); Si-free katoite—Lager et al. (1987).

* Shared octahedral edge.

** Unshared octahedral edge.

† Shared tetrahedral edge.

‡ Unshared tetrahedral edge.

§ Unshared dodecahedral edge.

‖ In cases where the unshared dodecahedral edge refined to values less than 2.75 Å, this distance was reset to 2.75 Å and assigned a weight of 1.0 in the calculation (Meagher, 1975).

with flexible polyhedra. The degree of flexibility of the polyhedra is determined by a weighting scheme based on crystal-chemical principles [refer to Burnham (1985) for review of weighting schemes]. Since the primary objective of this simulation was to determine how the garnet structure adjusts in response to tetrahedral expansion, the *d*–O distance (calculated from the vacancy or OH concentration) was assigned a high weight (1.0) in the least-squares refinement. The Ca–O and Al–O distances were weighted according to their valence bond strength, i.e., 0.25 and 0.50, respectively, whereas the O–O distances were assigned a relatively low weight (0.07). Prescribed cation-oxygen distances were calculated from the sum of ionic radii (Shannon and Prewitt, 1969). O–O distances were then computed from the cation-oxygen distance by assuming an undistorted polyhedron (Meagher, 1975). Since this model makes no assumptions about the distortions of individual polyhedra, the analysis should be relatively unbiased. The radius of the H atom was assumed to be 1.0 Å (Baur, 1972). The H atom was included in the calculation by specifying the four tetrahedral O–H distances (refer to Fig. 4) and the five H–H distances corresponding to the five different types of O–O distances. The short O–H distance (0.95 Å) was given a weight of 1.0; the remaining O–H (2.4Å) and H–H (2.0 Å) distances were given the same weight as O–O. Only distances were varied in the refinement; the unit-cell parameter was held constant. Observed unit-cell parameters were used except in those cases where they could be predicted from analytical expressions, e.g., equations of Novak and Gibbs (1971). The results of the calculations are presented in Table 10. The DLS simulation successfully predicts structural variations in the hydrogrossular series, e.g., the variation of shared versus unshared octahedral edges and the rate of change in the two Ca–O distances.

The DLS program was applied also to pyrope and andradite to learn more about the constraints imposed by the garnet structure on the extent of OH substitution (Table 10). With some basic assumptions about the expected length of interatomic distances, this information could

enable one to predict the structural "stability" of hydrogarnets as a function of X and Y cation radii and OH content. Novak and Gibbs (1971) used this approach to define a structural "stability" field for anhydrous garnets. In the present calculation, the unit-cell parameter for both garnets was estimated from the expression proposed by Basso et al. (1984a). Similar results, however, were obtained from refinements in which both atom coordinates and cell parameter were varied. The *d*–O distance was computed assuming the substitution of 4 OH and a tetrahedral-void size comparable to that determined for Si-free katoite (Lager et al., 1987).

As in hydrogrossular, the shared octahedral edge in the simulated hydroandradite structure (4 OH) is shorter than the unshared edge, i.e., the incorporation of structural OH causes a decrease in the shared edge relative to the unshared edge. The DLS structure for hypothetical hydropyrope is characterized by an extreme distortion of the Al octahedron. The shared and unshared octahedral edges are 2.58 and 2.85 Å versus 2.63 and 2.75 Å in the anhydrous DLS structure (Table 10). This distortion, coupled with the very short O–O distance (2.58 Å), may be a destabilizing feature of the hydropyrope structure and could explain the low-water contents thus far observed for these garnets (Aines and Rossman, 1985).

Garnets with substantiated high-water contents also have high grossular and/or andradite components. In the structures of grossular and andradite, the shared octahedral edge is longer than the unshared edge. This differs from the octahedral environment in pyrope where the shared edge is shorter than the unshared edge. Sacerdoti and Passaglia (1985) have suggested that the degree of hydration expected for a garnet may be related to the lengths of the shared and unshared octahedral edges in the anhydrous structure. The DLS calculations indicate that one effect of OH substitution is to decrease the length of the shared edge and increase the length of the unshared edge. One could argue therefore that as the length of the shared edge approaches some lower limit (presumably determined by the nonbonded interaction between oxygen atoms), the structure is unable to accommodate additional $(O_4H_4)^{4-} = (SiO_4)^{4-}$ substitution. This limit would be approached sooner in those garnets in which the shared edge is shorter than the unshared edge, e.g., pyrope and other aluminum silicate garnets with $r\{X\} < 1.01$ Å (Novak and Gibbs, 1971).

Zabinski (1966) also attempted to explain the high-water contents in grossular relative to other garnets. His arguments are based on a comparison of the mean cation-oxygen distance in the dodecahedron and the ionic radius of the eight-coordinated cation. The mean Ca–O distance in grossular suggests that Ca is too large for the dodecahedral cavity, e.g., the sum of ionic radii for $^{[8]}$Ca and $^{[4]}$O is 2.50 Å (Shannon and Prewitt, 1969) whereas the mean Ca–O distance in grossular is only 2.405 Å (Novak and Gibbs, 1971). Zabinski (1966) reasoned that the substitution of OH in the garnet structure would increase the size of the dodecahedron (Table 6) and provide a more energetically favorable environment for the Ca ion. In contrast, Mg is too small for the eight-coordinated site. Therefore, pyrope would theoretically "resist" OH substitution as this would cause an expansion of the dodecahedron and a destabilization of the structure.

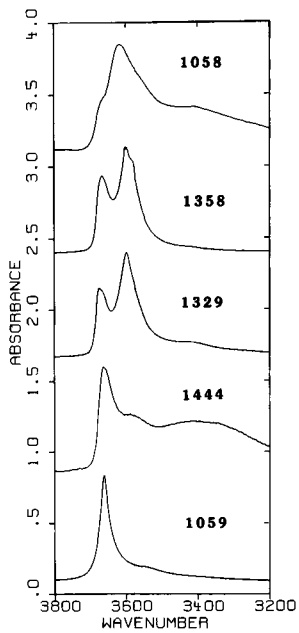

Fig. 6. Comparison of the infrared absorption spectra of natural and synthetic hydrogrossulars with high OH contents. From top to bottom: synthetic hibschite (1058, $x = 0.70$) in a KBr pellet; single-crystal plazolite from Crestmore, California (1358, $x = 1.47$); polycrystalline hibschite (1329, $x = 1.36$); katoite (1444, $x = 2.36$) in a KBr pellet; and synthetic Si-free katoite (1059) dispersed in a KBr pellet (G. R. Rossman, in preparation).

Figure 6 compares infrared spectra in the O–H stretch region for several natural and synthetic hydrogrossulars with high OH contents (Rossman, in preparation). Details of sample preparation and spectrophotometer measurements are described elsewhere (Aines and Rossman, 1985). Samples 1058 and 1059 refer to the H analogues of synthetic hibschite (this study) and Si-free katoite (Lager et al., 1987). The interesting feature of these spectra is the existence of two bands for the Si-containing garnets. Furthermore, in hibschite (1329, 1358, and 1058) and katoite (1444), these bands do not have the same intensity. The most prominent band in the katoite spectra is the 3662 cm^{-1} band of the synthetic Si-free end-member. As Si increases in the series from katoite to hibschite (1329), the intensity of the band at about 3598 cm^{-1} increases relative to the 3662 cm^{-1} band. A crude correlation exists between the relative intensities of the two OH bands for the intermediate solid-solution members and the O-site occupations in the disordered model.

The most straightforward interpretation of the IR spectra is that there is a linear superposition of two different spectral components that originate from two different OH environments. It is possible that vibrational coupling be-

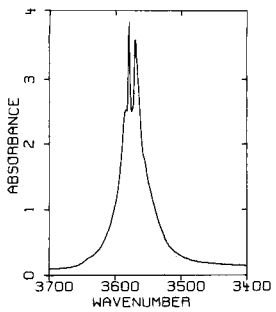

Fig. 7. Infrared absorption spectrum of single-crystal SB-3 in the wavenumber region 3400–3700 cm^{-1}. The reported water content is based on the integrated absorbance of the OH bands.

tween adjacent OH groups could give rise to more than one band. However, the single band observed for the Si-free end-member is not consistent with this interpretation. The fact that diffraction studies of hydrogrossulars indicate only one H position may reflect the resolution of the technique, i.e., the diffraction experiments reveal an average structure rather than local differences in the tetrahedral environment.

X-ray study of hydrous titanian andradite

Unit-cell parameters, site occupations, and water contents for the three andradite crystals are compared in Table 11. The substitution of OH in the garnet structure results in an expansion of the tetrahedra and a corresponding increase in the unit-cell parameter (Cohen-Addad et al., 1967). The larger unit-cell parameter of these garnets relative to that predicted for the anhydrous structure is consistent with the percentage of tetrahedral vacancies and the water contents derived from X-ray and IR techniques. The above results are also consistent with the variation in the tetrahedral *d*–O distance from 1.650(1) (sample SB-1) to 1.666(1) Å (sample SB-3) (Table 9). The longest Si–O distance observed in anhydrous silicate garnets is 1.655(2) Å (goldmanite) with a mean value of 1.65 Å in those structures with $r\{X\} > 1.0$ Å (Novak and Gibbs, 1971). These data confirm that the tetrahedral site is not fully occupied and that charge balance can be achieved by the substitution $(O_4H_4)^{4-} = (SiO_4)^{4-}$. There is no evidence to support a multisite OH substitution in andradites from this locality. With respect to Table 11, it should be noted that only in the case of sample SB-3 were X-ray and IR (Fig. 7) measurements carried out on the same single crystal. For crystals SB-1 and SB-2, which were lost during grinding, IR data obtained from crystals in the same thin section indicated two populations of andradites on the basis of water content (0.4 and 2.1 wt% H_2O). The IR water contents in Table 11 are based on an absolute calibration of spectra obtained from high-water grossulars (Rossman, in preparation). There is always some degree of uncertainty when calibration factors are applied to hydrogarnets with different compositions.

Table 11. Comparison of unit-cell parameters, site occupations, and water contents for San Benito (SB) andradites

	Unit-cell parameter (Å)		Site occupation		Wt% H_2O	
	Observed	Calculated*	Fe	Si	X-ray**	IR†
SB-1	12.057(2)	12.03	0.841(5)	0.960(5)	0.9	0.4
SB-2	12.085(2)	12.01	0.752(6)	0.915(5)	1.8	2.1
SB-3	12.106(2)	12.02	0.798(5)	0.860(5)	3.1	2.9

* Equations 3–5 of Novak and Gibbs (1971).
** X-ray = X-ray tetrahedral-site refinement.
† IR = integrated absorbance of OH band(s) from infrared absorption spectra.

Conclusions

1. The oxygen positional disorder in synthetic hibschite (Gr = 77%) can be described in terms of two oxygen sites (split-atom model) that are related by a small displacement along the tetrahedral *d*–O vector (Si–O vector in anhydrous silicate garnets). These sites correspond in position to the oxygen sites in grossular and Si-free katoite, end-members of the solid-solution series. The short O–D distance in hibschite, determined by neutron diffraction, is an artifact of the oxygen-ordered model.

2. The D positions in synthetic hibschite and Si-free katoite are similar, i.e., the D(H) position in the hydrogrossular series is not strongly dependent on OH content.

3. A simple geometric model (DLS) can be used to describe the structural changes in the hydrogrossular series, namely the differential rate of increase in the two Ca–O distances and the variation in the lengths of the shared and unshared octahedral edges.

4. The amount of OH in garnets appears to be structurally controlled. Those garnets [$r\{X\} > 1.0$ Å] in which the shared octahedral edge is longer than the unshared edge can incorporate more OH. Mantle garnets (rich in pyrope component) may contain only very limited amounts of water.

5. The tetrahedral site in the titanian andradites studied is not fully occupied (4–14% vacancies). The presence of OH in the structure suggests that charge balance can be achieved by the substitution $(O_4H_4)^{4-} = (SiO_4)^{4-}$. There is no evidence to support a multisite OH substitution.

Acknowledgments

G.A.L. acknowledges support of this research by the National Science Foundation (Experimental and Theoretical Geochemistry) through Grants EAR-8205605 and EAR-8719848. This work has benefited from the use of the Intense Pulsed Neutron Source at Argonne National Laboratory, which is funded by the U.S. Department of Energy, BES-Materials Science, under Contract W-31-109-ENG-38. Support from NSF Grant EAR-8618200 to G.R.R. is also acknowledged. R. Oberhänsli provided valuable assistance with the electron-microprobe analyses.

References cited

Aines, R.D., and Rossman, G.R. (1984) Water content of mantle garnets. Geology, 12, 720–723.

——— (1985) The hydrous component in garnets. I. Pyralspites. American Mineralogist, 69, 1116–1126.

Armbruster, Th., and Lager, G.A. (1989) Oxygen disorder and the hydrogen position in garnet-hydrogarnet solid solutions. European Journal of Mineralogy, in press.

Baerlocher, Ch., Hepp, A., and Meier, W.M. (1977) DLS-76: A program for the simulation of crystal structures by geometric refinement. Institute of Crystallography and Petrography. ETH, Zurich, Switzerland.

Basso, R., Della Giusta, A., and Zefiro, L. (1981) A crystal chemical study of a Ti-containing hydrogarnet. Neues Jahrbuch für Mineralogie Monatshefte, 230–236.

——— (1983) Crystal structure refinement of plazolite, a highly hydrated natural hydrogrossular. Neues Jahrbuch für Mineralogie Monatshefte, 251–258.

Basso, R., Cimmino, F., and Messiga, B. (1984a) Crystal chemistry of hydrogarnets from three different microstructural sites of basaltic metarodingite from Voltri massif (Western Liguria, Italy). Neues Jahrbuch für Mineralogie Abhandlungen, 148, 245–258.

——— (1984b) Crystal chemical and petrological study of hydrogarnets from a Fe-gabbro metarodingite (Gruppo di Voltri, Western Liguria, Italy). Neues Jahrbuch für Mineralogie Abhandlungen, 150, 247–258.

Baur, W.H. (1972) Prediction of hydrogen bonds and hydrogen atom positions in crystalline solids. Acta Crystallographica, B28, 1456–1465.

Birkett, T.C., and Trzcienski, W.E. (1984) Hydrogarnet: Multi-site hydrogen occupancy in the garnet structure. Canadian Mineralogist, 22, 675–680.

Burnham, C.W. (1985) Mineral structure energetics and modeling using the ionic approach. Mineralogical Society of America Reviews in Mineralogy, 14, 347–388.

Ceccarelli, C., Jeffrey, G.A., and Taylor, R. (1981) A survey of O–H···O hydrogen bond geometries determined by neutron diffraction. Journal of Molecular Structure, 70, 255–271.

Cohen-Addad, C., Ducros, P., and Bertaut, E.F. (1967) Etude de la substitution du groupement SiO_4 par $(OH)_4$ dans les composes $Al_2Ca_3(OH)_{12}$ et $Al_2Ca_3(SiO_4)_{2.16}(OH)_{3.36}$ de type grenat. Acta Crystallographica, 23, 220–230.

Coleman, R.G. (1986) Field trip guide book to New Idria area, California. 14th General Meeting of the International Mineralogical Association, Stanford University.

Dowty, E. (1971) Crystal chemistry of titanium and zirconium garnet. I. Review and spectral properties. American Mineralogist, 56, 1983–2009.

Dunitz, J.D., Schomaker, V., and Trueblood, K.N. (1988) Interpretation of atomic displacement parameters from diffraction studies of crystals. Journal of Physical Chemistry, 92, 856–867.

Enraf-Nonius. (1983) Structure determination package (SDP). Enraf-Nonius, Delft, The Netherlands.

Faber, J., Jr., and Hitterman, R.L. (1986) Neutron powder diffraction at a pulsed neutron source: A study of resolution effects. In C.S. Barrett, Ed., Advances in X-ray analysis, vol. 29, p. 119–130. Plenum Press, New York.

Foshag, W.F. (1920) Plazolite, a new mineral. American Mineralogist, 5, 183–185.

Hickmott, D.D., Shimizu, N., Spear, F.S., and Selverstone, J. (1987) Trace-element zoning in a metamorphic garnet. Geology, 15, 573–576.

Hill, R.J., and Howard, C.J. (1987) Quantitative phase analysis from neutron powder diffraction data using the Rietveld method. Journal of Applied Crystallography, 20, 467–474.

Huggins, F.E. (1977) Titanium-silicate garnets. II. The crystal chemistry of melanites and schorlomites. American Mineralogist, 62, 646–665.

Huggins, F.E., Virgo, D., and Huckenholz, H.G. (1977) Titanium-containing silicate garnets. I. The distribution of Al, Fe^{3+}, and Ti^{4+} between octahedral and tetrahedral sites. American Mineralogist, 62, 475–490.

International tables for X-ray crystallography. (1974) Vol. IV. Kynoch Press, Birmingham, England.

Jorgensen, J.D., Faber, J., Jr., Carpenter, J.M., Crawford, R.K., Haumann, J.R., Hitterman, R.L., Kleb, R., Ostrowski, G.E., Rotella, F.J., and Worlton, T.G. (1989) Electronically-focused time-of-flight powder diffractometers at the Intense Pulsed Neutron Source. Journal of Applied Crystallography, in press.

Justice, M., and Graham, E. (1982) The effect of water on the high-temperature deformation in olivine. Geophysical Research Letters, 9, 1005–1008.

Lager, G.A., Armbruster, Th., and Faber, J. (1987) Neutron and X-ray diffraction study of hydrogarnet $Ca_3Al_2(O_4H_4)_3$. American Mineralogist, 72, 758–767.

Lager, G.A., Armbruster, Th., Rotella, F.J., and Rossman, G.R. (1988) Structural and geometric refinements of hydrous garnets. Geological Society of America Abstracts with Programs, 17, 737.

Meagher, E.P. (1975) The crystal structures of pyrope and grossularite at elevated temperatures. American Mineralogist, 60, 218–228.

Novak, G.A., and Gibbs, G.V. (1971) The crystal chemistry of silicate garnets. American Mineralogist, 56, 791–825.

Pabst, A. (1937) The crystal structure of plazolite. American Mineralogist, 22, 861–868.

Passaglia, E., and Rinaldi, R. (1984) Katoite, a new member of the $Ca_3Al_2(SiO_4)_3$-$Ca_3Al_2(OH)_{12}$ series and a new nomenclature for the hydrogrossular group of minerals. Bulletin de Minéralogie, 107, 605–618.

Richardson, J.W., Jr., and Faber, J., Jr. (1986) Fourier-filtering techniques for the analysis of high-resolution pulsed-neutron powder-diffraction data. In C.S. Barrett, Ed., Advances in X-ray analysis, vol. 29, p. 143–152. Plenum Press, New York.

Rietveld, H.M. (1969) A profile refinement method for nuclear and magnetic structures. Journal of Applied Crystallography, 2, 65–71.

Rotella, F.J. (1986) User manual for Rietveld analysis of time-of-flight neutron powder-diffraction data at IPNS. Argonne National Laboratory, Argonne, Illinois.

Rotella, F.J., and Richardson, J.W. (1986) The IPNS Rietveld analysis software package for time-of-flight powder-diffraction data: Recent developments. Institute of Physics Conference Series, 81, 27–36.

Sacerdoti, M., and Passaglia, E. (1985) The crystal structure of katoite and implications within the hydrogrossular group of minerals. Bulletin de Minéralogie, 108, 1–8.

Schomaker, V., and Marsh, R.E. (1983) On evaluating the standard deviation of U_{eq}. Acta Crystallographica, A39, 819–820.

Schwartz, K.B., Nolet, D.A., and Burns, R.G. (1980) Mössbauer spectroscopy and crystal chemistry of natural Fe-Ti garnets. American Mineralogist, 65, 142–153.

Sears, V.F. (1986) Neutron scattering in condensed matter research. In K. Skold and D.L. Price, Eds., Methods of experimental physics, vol. 23, part A, p. 521. Academic Press, Orlando, Florida.

Shannon, R.D., and Prewitt, C.T. (1969) Effective ionic radii in oxides and fluorides. Acta Crystallographica, B25, 925–946.

Von Dreele, R.B., Jorgensen, J.D., and Windsor, C.G. (1982) Rietveld refinement with spallation neutron powder-diffraction data. Journal of Applied Crystallography, 15, 581–589.

Waychunas, G.A. (1987) Synchrotron radiation XANES spectroscopy of Ti in minerals: Effect of Ti bonding distances, Ti valence, and site geometry on absorption edge structure. American Mineralogist, 72, 89–101.

Zabinski, W. (1966) Hydrogarnets. Polska Akademia Nauk, Oddzial Krakowie, Komisja Nauk Mineralogicznych, Prace Mineralogiczne, 3, 1–69.

Zucker, U.H., Perenthaler, E., Kuhs, W.F., Bachmann, R., and Schulz, H. (1983) PROMETHEUS: A program system for investigation of anharmonic thermal vibrations in crystals. Journal of Applied Crystallography, 16, 358.

Manuscript received August 8, 1988
Manuscript accepted March 7, 1989